coatings

MDPI

Article

Effect of Chloride Salt Erosion on the Properties of Straw Fiber Reactive Powder Concrete

Hangyang Wang [1,2], Kaiwei Gong [1,2], Bingling Cheng [3], Xi Peng [2,4,*], Hui Wang [1,*] and Bin Xu [4]

[1] School of Civil Engineering and Geographical Environment, Ningbo University, Ningbo 315000, China; 1105390194@aliyun.com (H.W.); 1095957844@aliyun.com (K.G.)
[2] School of Civil Transportation Engineering, Ningbo University of Technology, Ningbo 315211, China
[3] Ningbo Yonghuan Yuan Environmental Protection Engineering Technology Co., Ltd., Ningbo 315000, China; 263454376@aliyun.com
[4] Ningbo Roaby Technology Industrial Group Co., Ltd., Ningbo 315800, China; 5632374376@aliyun.com
* Correspondence: pengxi@nbut.edu.cn (X.P.); huiwang123@aliyun.com (H.W.)

Abstract: Straw fibers are renowned for their cost-effectiveness, sustainability, and durability. They represent a promising natural reinforcement option for reactive powder concrete (RPC). This paper investigated the impact of straw fibers on RPC's workability, mechanical performance (mechanical strength and flexural toughness), and electrical properties (electrical resistance and AC impedance spectroscopy curves). The straw fiber volumes ranged from 1% to 4.0% of the total RPC volume. Specimens were cured under standard curing conditions for 3, 7, 14, and 28 days. Mechanical and electrical properties of the specimens were tested before chloride salt erosion. The mass loss and ultrasonic velocity loss of the samples were measured under NaCl freeze–thaw cycles (F-Cs). The mass loss, ultrasonic velocity loss, and mechanical strengths loss of the samples were measured under NaCl dry–wet alternations (D-As). The findings indicated that incorporating straw fibers enhanced RPC's flexural strength, compressive strength, and flexural toughness by 21.3% to 45.76%, −7.16% to 11.62%, and 2.4% to 32.7%, respectively, following a 28-day curing period. The addition of straw fibers could augment the AC electrical resistance of the RPC by 10.17% to 58.1%. The electrical characteristics of the RPC adhered to series conduction models. A power function relationship existed between the electrical resistance and mechanical strengths of the RPC. After 10 NaCl D-As, the mass loss rate, ultrasonic velocity loss rate, flexural strength, and compressive strength loss rates of the RPC decreased by 0.42% to 1.68%, 2.69% to 6.73%, 9.6% to 35.65%, and 5.41% to 34.88%, respectively, compared to blank samples. After undergoing 200 NaCl F-Cs, the rates of mass loss and ultrasonic velocity loss of the RPC decreased by 0.89% to 1.01% and 6.68% to 8.9%, respectively.

Keywords: straw fibers; reactive powder concrete; chloride salt erosion; mechanical performance; electrical properties

check for updates

Citation: Wang, H.; Gong, K.; Cheng, B.; Peng, X.; Wang, H.; Xu, B. Effect of Chloride Salt Erosion on the Properties of Straw Fiber Reactive Powder Concrete. *Coatings* **2024**, *14*, 1069. https://doi.org/10.3390/coatings14081069

Academic Editor: Günter Motz

Received: 30 July 2024
Revised: 17 August 2024
Accepted: 19 August 2024
Published: 21 August 2024

Copyright: © 2024 by the authors. Licensee MDPI, Basel, Switzerland. This article is an open access article distributed under the terms and conditions of the Creative Commons Attribution (CC BY) license (https://creativecommons.org/licenses/by/4.0/).

1. Introduction

Ordinary concrete is a fundamental material in civil engineering, appreciated for its cost-effectiveness and ease of construction. It is widely used in coastal infrastructure projects, including bridges, tunnels, harbors, and waterways [1]. However, under challenging service conditions and heightened standards for specialized projects [2–4], conventional concrete often fails to meet project requirements [5–7]. It is imperative to find a new concrete material.

Reactive powder concrete (RPC), a novel cementitious composite, offers exceptional mechanical properties and durability [8–13]. Originating in the 1990s through Bouygues Corporation's innovation [14], RPC is designed to maximize particle packing density. Precast RPC components have been extensively utilized in engineering projects [15–18], enhancing the longevity of offshore concrete structures. Scholars, including Blunt [19], advocate for fiber reinforcement as an optimal solution to enhance crack control in concrete

structures exposed to harsh erosive environments. The commonly used fibers are steel fibers, synthetic fibers, and basalt fibers. For instance, studies by P.R. et al. showed that RPC with 2% fiber content exhibits ductility 5.21 times greater than that of fiberless specimens. Steel fibers enhance both ductility and residual load-carrying capacity of the RPC [20]. A study by Hiremath et al. indicated that RPC with 0.1% polypropylene and polyester fibers demonstrates good spalling resistance, while a 0.5% fiber dosage enhances residual mechanical and durability properties at elevated temperatures [21]. Wang et al. demonstrated that incorporating 1.2% oriented steel fibers with an aspect ratio of 150 significantly enhances flexural and compressive strengths, as well as bending toughness [22]. Branston et al. demonstrated that incorporating BF enhanced the initial crack resistance of concrete under flexural loading [23]. However, the high cost of steel fibers represents a significant barrier to their widespread adoption in construction projects. Synthetic fibers have a serious effect on concrete flow and steel fiber corrosion. Basalt fibers have strict requirements on the composition of the raw ore [24].

As global environmental awareness grows, the engineering field faces increasingly stringent requirements regarding carbon emissions. Straw fiber is one of the abundant natural fibers and a major by-product of agriculture. In China, nearly 900 million tons of straw are produced annually, with the majority being disposed of by burning. This practice not only pollutes the environment but also results in a significant waste of resources [25,26]. Straw fibers offer several advantages as a natural material: they are lightweight, renewable, extremely tough, and easy to manufacture [27,28]. The use of straw fibers has been shown to improve the mechanical strength of concrete [29]. It also helps to reduce the overall dead weight of the concrete [30]. For example, Wu et al. showed that incorporating CSF (corn straw fiber) moderately enhances the compressive strength, flexural strength, and cracking toughness of EPS concrete [31]. Additionally, these fibers promote the formation of denser hydration products, enhancing crack repair and increasing permeability [32]. This approach not only improves the structural integrity of concrete, but also its durability under various conditions [33]. At present, a considerable number of scholars have conducted in-depth studies on the performance mechanisms of various types of straw fiber, such as rice straw fiber, corn straw fiber, and highland barley straw fiber, in different concrete materials [34–36]. However, the performance of straw fiber RPC under conditions of chloride salt attack remains an area that has not been sufficiently explored.

This study focused on investigating the effects of chloride salt erosion on the performance of straw fiber RPC. Before chloride salt erosion, the feasibility and excellence of incorporating straw fibers into RPC were validated through tests of workability, mechanical properties, and electrochemical performance. After chloride salt erosion, the defects within RPC and changes in its performance were detected through mass, ultrasonic, and mechanical strength loss experiments. In addition, the mechanical strength of the straw fiber RPC was characterized by electrical performance. The results of this study will provide a benchmark for the use of straw fiber RPC in chloride salt erosion environments and will also aid in developing specialized methods to predict future performance.

2. Experimental

2.1. Materials and Sample Preparation

2.1.1. Materials

The research utilized ordinary Portland cement (OPC) obtained from Jiangsu Huaxi Cement Manufacturing Co., Ltd., based in Wuxi, China. This OPC demonstrates a specific surface area of 350 m^2/kg and a density of 3.0 g/cm^3. The OPC displayed initial and final setting times of 121 min and 233 min, respectively. Silica fume (SF), boasting a density of 2.2 g/cm^3 and a specific surface area measuring 15 m^2/g, and containing over 98% SiO_2, was utilized as an additional cementitious component. Quartz sand (QS) was employed as the aggregate, consisting of three particle sizes: 1~0.71 mm, 0.59~0.35 mm, and 0.15~0.297 mm. The mass ratio of coarse, medium, and fine sands was 1:1.5:0.8. QS and SF were manufactured at Lingshou Xinhui Mining Processing Factory, Shijiazhuang, China. We

utilized a polycarboxylate-based superplasticizer (SP) manufactured by Shanghai Yingshan New Material Technology Co., Ltd., Shanghai, China. The tawny microemulsion solution exhibited a 40% water-reduction capability. Additionally, we employed a defoamer known as DF-04. The defoamer was a polyether-based surfactant comprising a mixture of dry powder carriers, which are white or light grey in color, with a density of 300–450 g/L and a pH of 7.0–7.5. The two additives in question were manufactured by Shanghai Yingshan New Materials Technology Co., Ltd., Shanghai, China. The straw fibers, with a density of 27 kg/m^3, were obtained from Jiangsu Fangyuan Tong Biotechnology Co., Ltd., Sucheng, China. The fiber lengths exhibited a range of 1 mm to 20 mm. The primary chemical constituents of straw fiber were quite similar, predominantly including cellulose, hemicellulose, and lignin. The physical diagram of straw fibers is shown in Figure 1. The chemical compositions of OPC, QS, and SF are presented in Table 1 for reference.



Figure 1. The physical diagram of straw fibers.

Table 1. Chemical composition of raw materials (%).

Type	Chemical Composition/%							
	SiO_2	Al_2O_3	Fe_2O_3	MgO	CaO	SO_3	R_2O	SiO_2
OPC	20.86	5.47	3.94	1.73	62.23	2.66	0.48	20.86
QS	34.06	14.74	0.83	9.73	35.93	0.23	3.51	34.06
SF	90	0.8	0.6	0.8	0.4	0	7.4	90

2.1.2. Sample Preparation

The experiment was conducted using a 3 L volume to prepare the mixture proportion, as illustrated in Table 2. All materials were weighed using an electronic balance. The particulate-sized quartz sand, silica fume, and Portland cement were successively introduced into a pre-wetted UJZ-15 mortar mixer. The mixing time was set at eight minutes, after which the mixer was initiated. After mixing for 30 s, a blend of water, a water-reducing agent, and a defoamer was gradually introduced. The duration was then noted to determine the setting time of the sample. One minute after commencing the mixing process, the addition of straw fibers was undertaken in order to achieve uniform mixing. Upon completion of the mixing process, the machine automatically ceased operation, and the resulting concrete slurry exhibited satisfactory flowability, indicating that it was ready for casting specimens. The RPC mixture from the mixer was poured into prism-shaped specimens of dimensions 40 × 40 × 160 mm^3 and 50 × 50 × 50 mm^3, with stainless steel mesh inserted on both sides (size 45 × 60 mm^2) and covered with plastic film. Each group was labeled and placed in a SHBY-40B standard constant temperature and humidity curing chamber at a temperature of 20 ± 2 °C and humidity above 95% for a period of 24 h. Following the curing period, the molds were removed and each specimen was correctly labeled. The production process is illustrated in Figure 2.

Table 2. Mass (kg/m^3) and mass ratio of proportioned fresh cement paste.

Materials	Water	OPC	SF	QS	Water Reducer	Defoamer	Straw Fibers
1	339.6	1018.9	339.6	679.2	26.4	1.32	0
2	339.6	1018.9	339.6	679.2	26.4	1.32	27
3	339.6	1018.9	339.6	679.2	26.4	1.32	54
4	339.6	1018.9	339.6	679.2	26.4	1.32	81
5	339.6	1018.9	339.6	679.2	26.4	1.32	108
mass ratio	14.12%	42.36%	14.12%	28.24%	1.09%	0.05%	

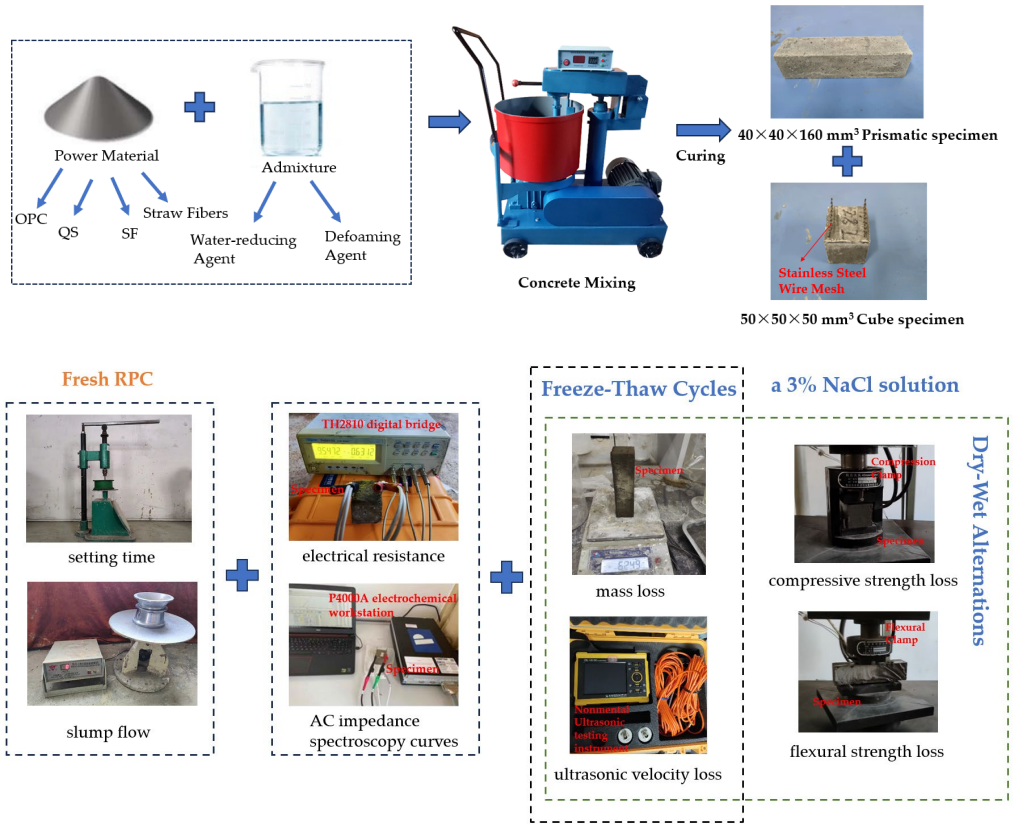


Figure 2. Preparation and experimental procedure of straw fiber RPC.

2.2. Chloride Salt Environments

Concrete test blocks were immersed in a 3% NaCl solution for 4 days after a standard curing period of 24 days. Following this, samples were placed into a rapid freeze–thaw machine from Tianjin Gangyuan Test Instrument Factory (Tianjin, China) for conducting the rapid freeze–thaw test. Concrete test blocks were exposed to temperatures spanning from −15 °C to 8 °C within plastic sleeves filled with a 3% NaCl solution during the experiment. Each freeze–thaw cycle extended over a period of 3 h, comprising 2 h of freezing followed by 1 h of thawing. A total of 200 cycles were conducted on the samples during the F-Cs test, with measurements of the mass and ultrasonic velocity taken at 50-cycle intervals. The NaCl D-As were assessed using a cyclic salt spray tester produced by Jiangsu Jiuyi Power Equipment Co., Ltd., Yangzhou, China. Following each five-alternation interval, the mass, ultrasonic velocity, and strength of the specimens were measured. Each cycle of D-As spanned 48 h, commencing with drying specimens free of surface moisture at 80 °C for 36 h, succeeded by a 2 h cooling phase. Subsequently, the cooled specimens underwent a 10 h immersion in NaCl solution prior to measurements, maintaining consistent conditions throughout the brief measurement procedure.

2.3. Measurement Method

2.3.1. Slump Flow and Setting Time Experiments

According to the Chinese standard GB/T 2419-2005 for measuring the fresh RPC slump flow [37], the procedure entailed cleaning the tabletop, tamping bar, and molds with a wet cloth. Subsequently, the fresh RPC was poured in two layers into the testing molds, with each layer tamped 15 times with a rod. Subsequently, the mold was elevated vertically and subjected to 25 vibrations using an electric vibrating table. Subsequently, the maximum and perpendicular diameters were measured and averaged to determine the slump flow. The setting time was determined using a ZKS-100 pointer device. This device was produced by Hebei Xin Test Machine Manufacturing Co., Ltd., Cangzhou, China, and the procedures followed were by the ASTM C191-19 [38]. The cement paste was poured into the mold. The Vicat needle was positioned above the surface and slowly inserted vertically into the paste. The time at which the needle first contacted the surface was recorded as the initial setting time. For the final measurement, the needle was inserted until it could no longer penetrate the paste, and this time was recorded as the final setting time.

2.3.2. Mechanical Property Experiments

The assessment of mechanical strength was conducted using the YAW-300D microcomputer automatic cement compression and folding testing machine. This machine is produced by Jinan Liling Testing Machine Co., Ltd., Jinan, China. Specimens measuring $40 \times 40 \times 160$ mm^3 were subjected to testing for flexural strength, compressive strength, and flexural toughness in accordance with the Chinese standard GB/T17671-1999 [39]. The loading rates employed were 0.05 kN/s for flexural strength and 2.4 kN/s for compressive strength. The displacement at the mid-bottom of the specimen was recorded using the CMT 5205 microcomputer-controlled electronic universal testing machine produced by Zhengzhou Muchen Automation Technology Co., Ltd., Zhengzhou, China, along with a linear variable displacement transducer (LVDT). The loading rate employed was 0.05 mm/min for the flexural toughness. The flexural toughness was determined by integrating the initial segment of the bending force-displacement curve from the peak load point during flexural strength testing. The precise measurement procedures were outlined in Ref. [40]. The methodology employed for the assessment of flexural toughness is illustrated in Figure 3.

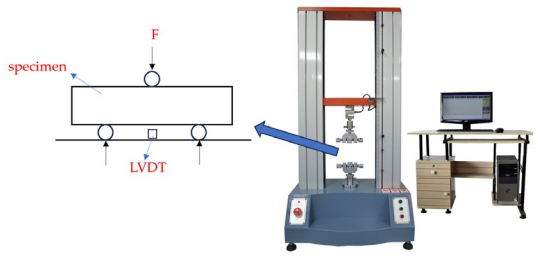


Figure 3. Flexural toughness test of the RPC.

2.3.3. Compactness Experiments

This study utilized the ZBL-U5100 ultrasonic testing instrument. It was manufactured by Beijing Zhibolian Technology Co., Ltd., Beijing, China. According to ASTM C597-1, both sides of the test block were first cleaned, and petroleum jelly was uniformly applied to both sides of the sample to ensure good ultrasonic transmission [41]. Two metal probes were then positioned close to the axis on both sides of the sample, and the propagation time of ultrasonic waves in the concrete was recorded. After all steps were completed, the ultrasonic velocity was calculated based on the measured propagation time.

2.3.4. Electrical Performance Test

According to ASTM C57, the electrical resistance of the sample was tested using a two-electrode method. Two electrodes, composed of 316 L stainless steel mesh with an

aperture of 4 mm and spaced 40 mm apart, were connected to the surface of the concrete specimen [42]. The electrical resistance was measured utilizing a TH2810 digital bridge (Changzhou Tonghui Co., Ltd., Changzhou, China) at a constant frequency of 10 kHz and a voltage of 1 V. The AC impedance spectrum was determined using the P4000A electrochemical workstation provided by AMETEK Trading (Shanghai) Co., Ltd., Shanghai, China, which operated between frequencies of 10^5 Hz and 1 Hz and within a voltage range of −10 mV to 10 mV [43,44].

3. Results and Discussions

3.1. Slump Flow and Setting Time Analysis

The impact of straw fibers on the slump flow and setting time of the RPC is illustrated in Figures 4 and 5. As the proportion of straw fiber content increased, the slump flow of the RPC initially decreased, then increased, and subsequently gradually decreased. Compared to the blank specimens, the RPC showed a slump flow reduction of 9.8%~13.1%. This phenomenon can be explained by two main factors. First, with a constant water–cement ratio, the significant water absorption of straw fibers reduces the water available to the cementitious material, thereby decreasing the fluidity of the RPC and, consequently, the slump flow. Second, adding straw fibers results in the formation of a spatial mesh structure within the RPC. The mechanical interlocking of straw fibers and matrix increases the friction within the RPC, reducing its fluidity and consequently the slump flow. However, silica fume forms agglomerates during the mixing process. Following the addition of straw fibers, these agglomerates disintegrate into fine particles, increasing the fluidity of the concrete [45].

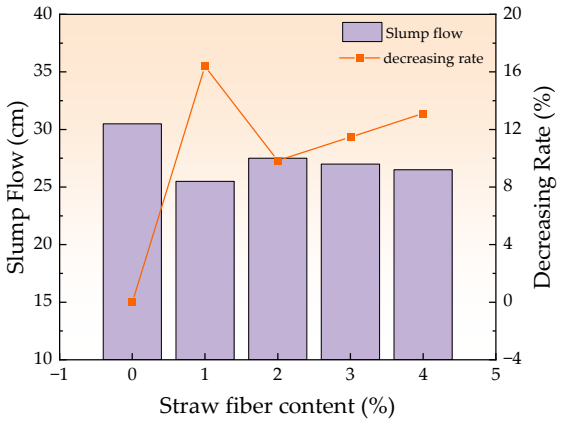


Figure 4. The impact of straw fibers on the slump flow of the RPC.

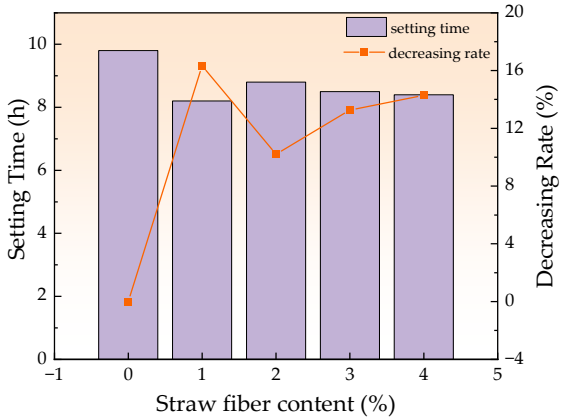


Figure 5. The impact of straw fibers on the setting time of the RPC.

Additionally, incorporating straw fibers has been shown to promote the setting time of the RPC. With an increase in straw fiber content, the setting time initially decreases, then increases, and finally stabilizes. Compared to the blank specimens, the setting time of the RPC decreased by 10.2%~16.3%. This phenomenon can be explained by two main factors. First, the straw fibers have developed a relatively cohesive spatial network structure within the RPC, characterized by substantial mechanical interlocking and frictional forces. This has notably accelerated the initial setting rate of the RPC. Second, the dissolution of hemicellulose and other substances present in straw fibers in alkaline environments prevented the initial setting of cement [46].

3.2. Mass Loss Analysis

Figure 6 depicts the mass loss rates of RPC following various cycles of NaCl D-A and F-C. In the RPC specimens containing 1%, and 3% straw fibers, a gradual increase in the mass loss rate was observed during the dry–wet alternations. Conversely, the RPC specimens doped with 2% and 4% straw fibers initially showed an increase followed by a decrease in mass loss rates during the alternating dry–wet alternations. The concrete spalling observed on the specimen surface was a consequence of the contraction and expansion of the specimen during the alternating wet and dry cycles. Moreover, the initial products were observed to be encapsulated on the surface of the cement particles, and the water did not react sufficiently with the cement particles. This consequently affects the hydration of the concrete. Consequently, the mass of the product is considerably less than that of the spalled material, resulting in a reduction in the overall mass of the specimen. The immersion of the specimen in brine over an extended period of time results in a chemical reaction between the salt and substances such as tricalcium chlorate, leading to the formation of calcium chloroaluminate polycrystalline materials and an increase in specimen mass [47]. During F-Cs, the reduction in specimen mass is attributable to stress-induced fissures caused by moisture freezing, while the increase may be linked to secondary hydration of the cementitious material and crystal formation through chloride salt erosion [48]. After undergoing 10 cycles of D-A and 200 F-Cs using an NaCl solution, the incorporation of straw fibers resulted in decreased mass loss rates of the RPC, ranging approximately from 0.42% to 1.68% and 0.89% to 1.01%.

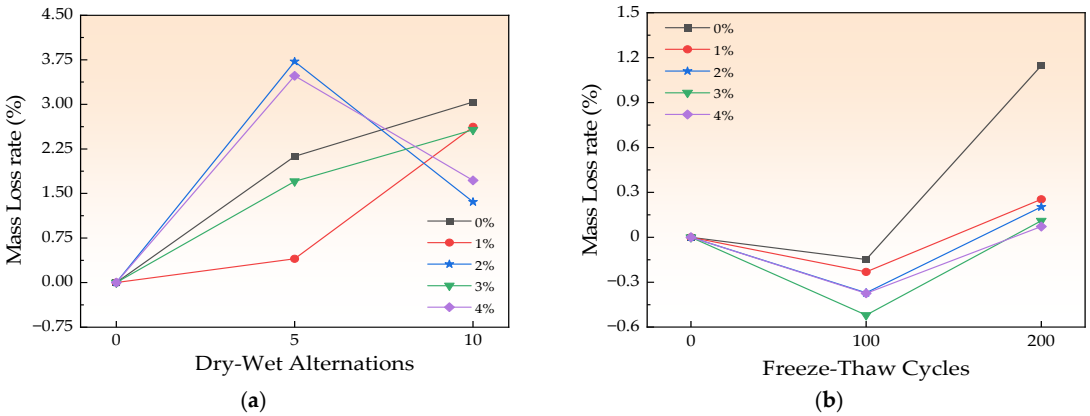


Figure 6. The mass loss rate after different numbers of NaCl D-As and F-Cs: (**a**) D-As; (**b**) F-Cs.

3.3. Ultrasonic Velocity Loss Analysis

Figure 7 depicts the ultrasonic velocity and attenuation rate of the RPC following various cycles of NaCl D-As and F-Cs. Ultrasonic velocity showed a declining trend as fiber content increased during the initial NaCl D-As. This could be attributed to the hollow and porous structure of straw fibers. The inclusion of straw fibers in RPC samples increases the internal porosity, which in turn reduces the density of the samples [49]. In the initial five cycles of NaCl D-As, the RPC specimens without straw fibers exhibited significantly

greater ultrasonic velocity loss compared to those with straw fibers. This occurs because even minimal quantities of straw fibers can serve as fillers. Strong chemical bonds and mechanical interlocking are formed by the straw fibers with the cement matrix, thereby enhancing the density of the samples [50]. Between cycles 5 to 10 of D-As, the erosion damage to the specimens tends to stabilize. As the number of F-Cs increased, the ultrasonic velocity of the specimens without straw fibers exhibited a notable initial increase, followed by a subsequent decrease. This pattern mirrors the mass loss under freeze–thaw conditions discussed in Section 3.2. The average velocity trend remains stable across increasing F-Cs when straw content is between 1% and 4%. After 10 NaCl D-As and 200 NaCl F-Cs, the addition of straw fibers led to a reduction in ultrasonic velocity loss rates of the RPC, ranging from 2.69% to 6.73% and 6.68% to 8.9%, respectively. At 2% straw fiber content, the specimens are least affected by chloride salt erosion, and changes in internal density are minimal.

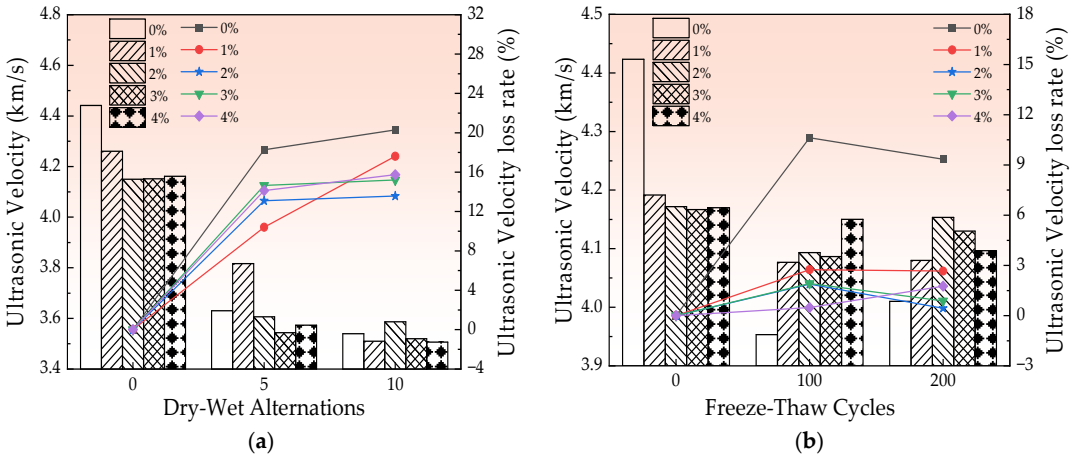


Figure 7. The ultrasonic velocity after different numbers of NaCl D-As and F-Cs: (**a**) D-As; (**b**) F-Cs.

3.4. Mechanical Strength Analysis

Figure 8 presents the RPC samples' mechanical strengths across varying curing times. The figures show that incorporation of an optimal quantity of straw fibers has been demonstrated to enhance the flexural and compressive strengths of the RPC at both the early and late stages of the material's curing. After 7 days of curing, the incorporation of straw fibers resulted in a 7.2% to 26.7% increase in flexural strength of the RPC and a −6.17% to 8.43% increase in compressive strength of the RPC. The addition of straw fibers increased the flexural and compressive strengths of the RPC by 21.3% to 45.76% and −7.16% to 11.62%, respectively, after curing for 28 days. A 2% straw fiber content represents the optimal ratio for achieving maximum flexural and compressive strengths of the RPC. However, increasing the straw fiber content to 3% and 4% led to a reduction in compressive strength of the specimens compared to specimens without straw fibers. This result can be attributed to two factors: Firstly, straw fibers, characterized by a hollow and porous structure, can cause aggregation when present in excessive amounts in concrete. These issues may lead to internal defects in RPC, thereby creating points of weakness [29]. Secondly, straw fibers, with their high water absorption capacity, can absorb excessive free water during the concrete's hydration process. This interference with the concrete's normal hydration can subsequently reduce the compressive strength of the samples [51].

Figure 9 illustrates the cumulative loss of flexural and compressive strengths in RPC specimens with varying straw fiber contents under D-A conditions. Both straw fiber content and the number of D-As considerably influence RPC's strength. As the number of D-A cycles increases, RPC's strength loss initially increases and then stabilizes. After 10 NaCl D-As, adding straw fibers reduced the loss rates of flexural and compressive strengths of the RPC by 9.6%~35.65% and 5.41%~34.88%, respectively, compared to blank samples.

This phenomenon is attributable to two factors: Under D-A conditions, incorporating straw fibers into RPC leads to secondary hydration of the material, resulting in more new cementitious gel formation. Additionally, stresses generated by the alternating dry and wet conditions, due to drying shrinkage and temperature variations, lead to the enlargement of internal pores within the samples. These horizontal stresses are effectively counteracted by straw fibers, which improve the structural stability and significantly reinforce the samples. According to M.S. Ammari et al., straw displays remarkable ductility, which further enhances the mechanical properties of concrete [52]. Following 10 NaCl D-As, RPC specimens with 2% straw fibers showed the lowest levels of flexural and compressive strength loss. Figure 10 displays the images of specimens both before and after exposure to chloride salt erosion under experimental loads, which led to their failure. The failure mode in the RPC specimens experiencing flexural failure was characterized by complete fracture. Compared to specimens containing 2% fiber, those without fibers exhibited significantly larger crack widths. This observation clearly demonstrates that the incorporation of straw fibers inhibits concrete fracturing and spalling.

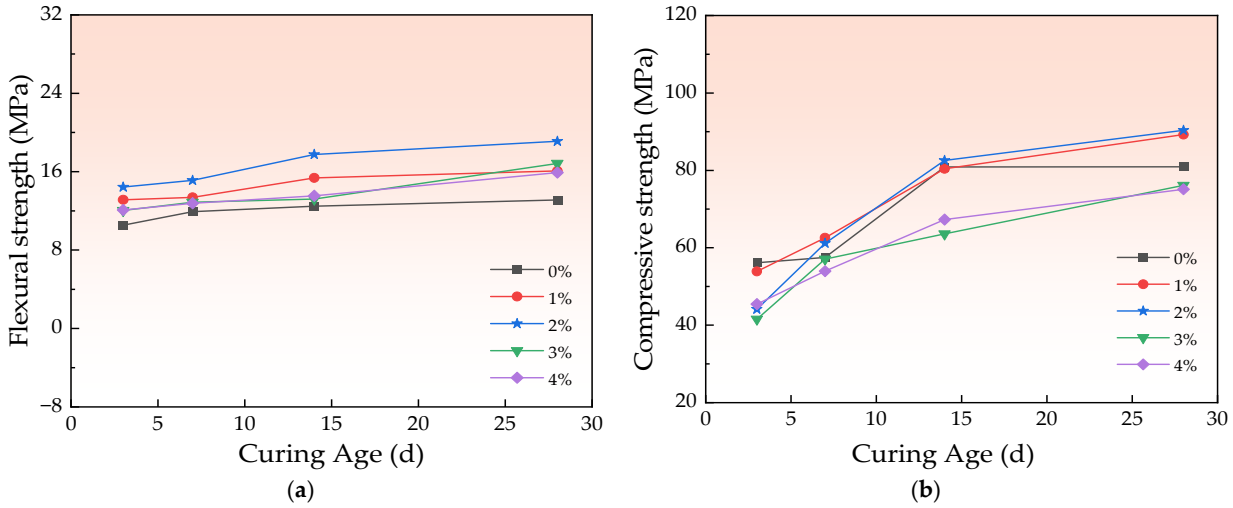


Figure 8. (**a**) Flexural strength of the RPC over different curing periods; (**b**) compressive strength of the RPC contents over different curing periods.

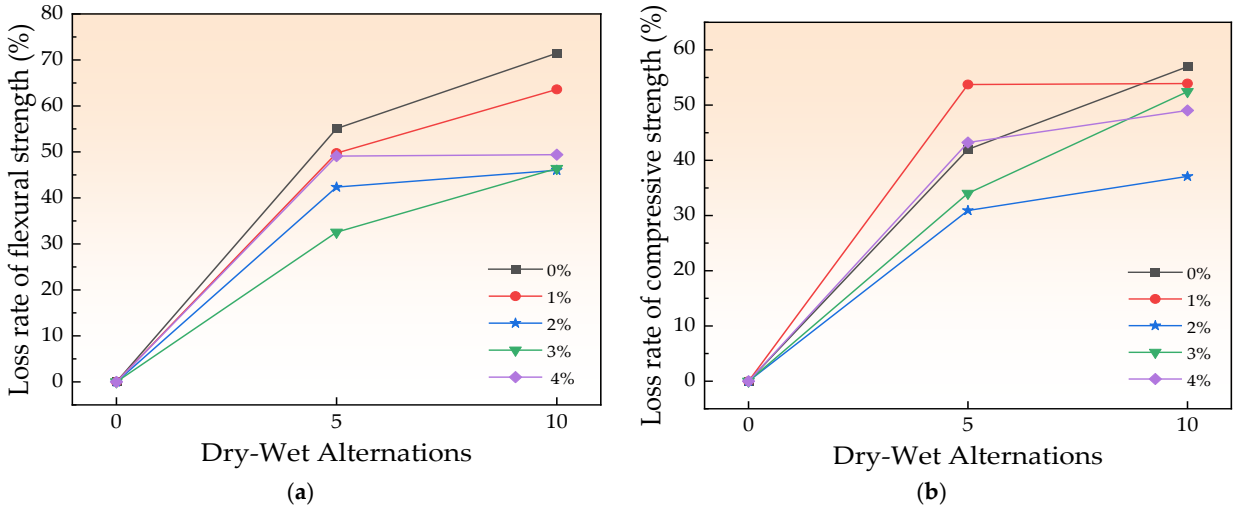


Figure 9. (**a**) The cumulative loss of flexural strength of the RPC under D-As; (**b**) the cumulative loss of compressive strength of the RPC under D-As.

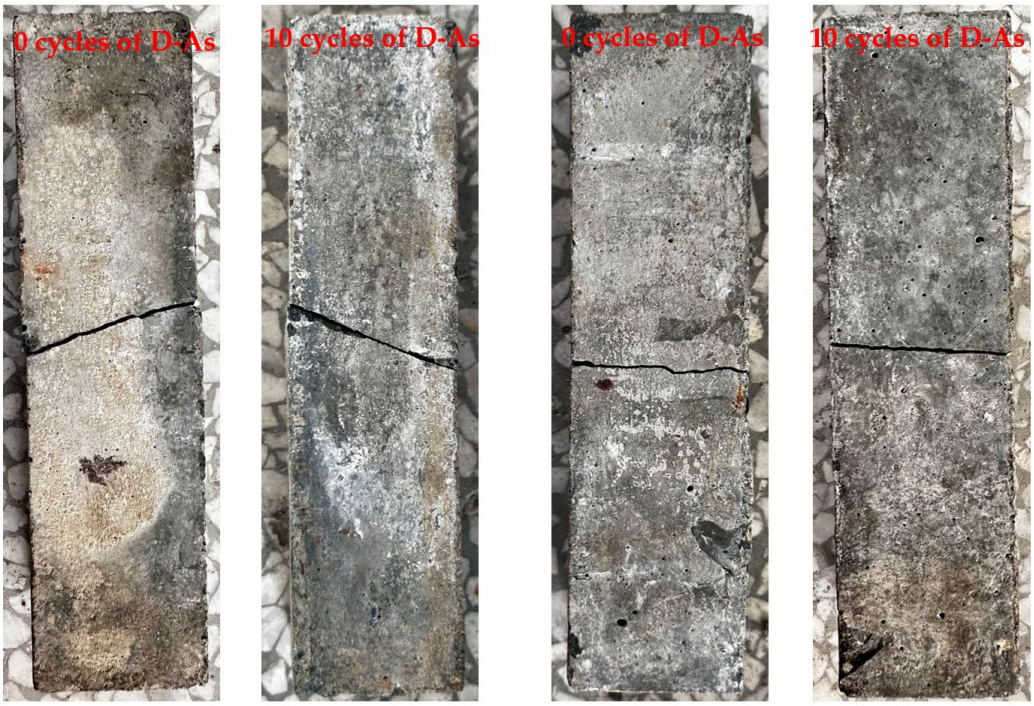


Figure 10. Images of specimens failing under experimental loading before and after chloride salt attack.

3.5. Flexural Toughness Analysis

Figure 11 illustrates the flexural load and displacement curves of the RPC at different curing ages. The graph shows that during the RPC flexural strength test, the force–displacement curve initially developed horizontally. As displacement increased, the force on the RPC specimen gradually increased until reaching the maximum flexural failure load. Ultimately, the specimen abruptly fractured and the force dropped to zero. Although the basic trend of each group's test curve was similar, the curves exhibited fluctuations. This phenomenon can be attributed to the rough edges of the RPC specimens and incomplete contact with the loading machine, resulting in uneven force distribution during the testing process, resembling peak-like patterns [53].

Figure 12 illustrates the impact of curing age on the flexural toughness of the RPC. The graph shows that flexural toughness initially increased and then decreased as straw fiber content increased. After 7 days of curing, straw fibers increased flexural toughness of the RPC by 3.36%~13.6%. Following 28 days of curing, the flexural toughness of the test blocks reached its peak at a 2% fiber content, exhibiting a 32.7% increase compared to the control group. Straw fibers' bridging effect in concrete can enhance the material's toughness and tensile strength. Furthermore, straw fibers can absorb and disperse stress around cracks, delaying crack propagation and enhancing crack resistance. However, increasing the straw fibers may cause excessive internal voids and defects in the concrete, resulting in lower compressive strength of the concrete. This can result in early deterioration of the concrete under external loads, leading to decreased concrete toughness [54].

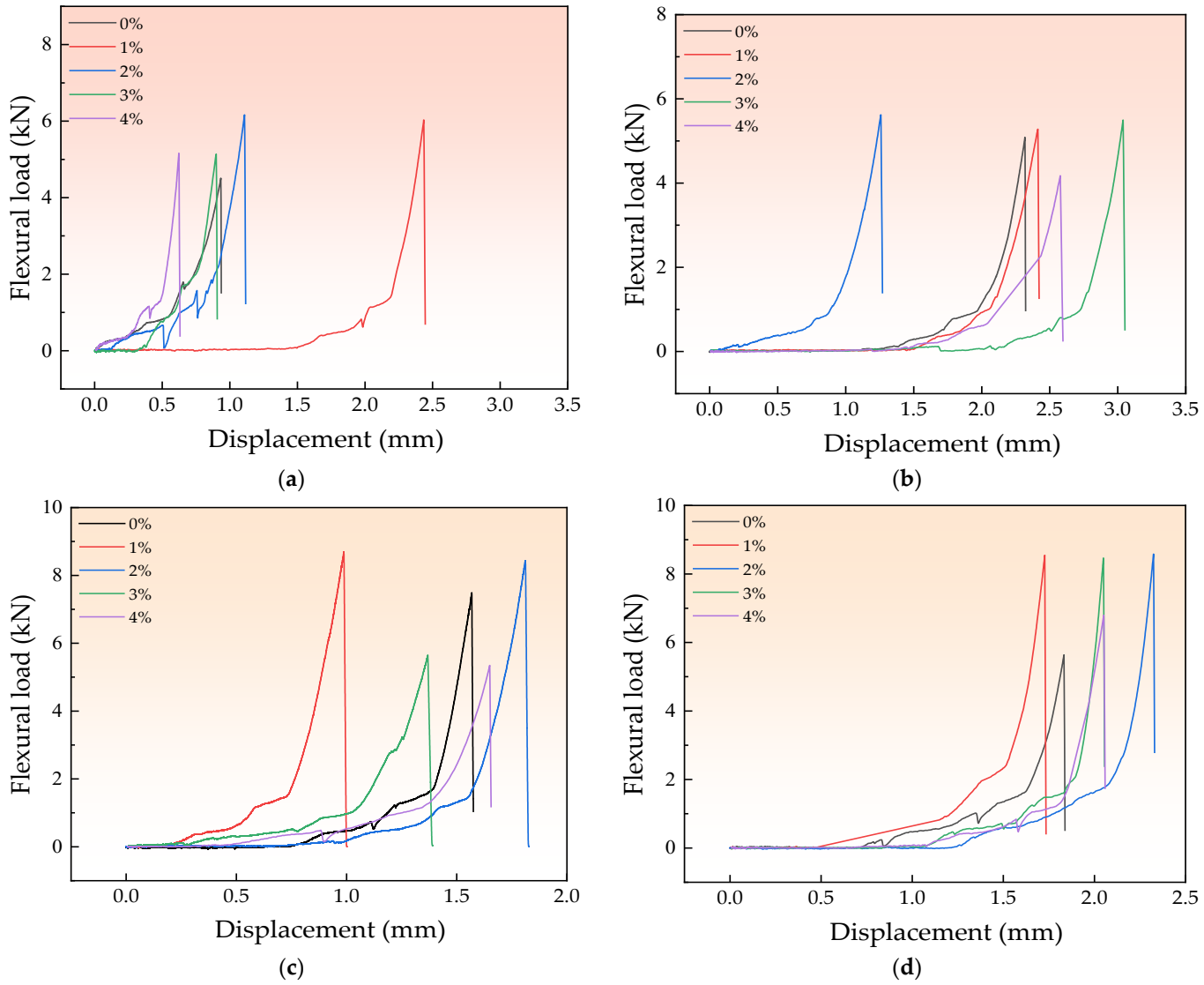


Figure 11. Flexural load and displacement of the RPC at different curing ages: (**a**) 3 d; (**b**) 7 d; (**c**) 14 d; (**d**) 28 d.

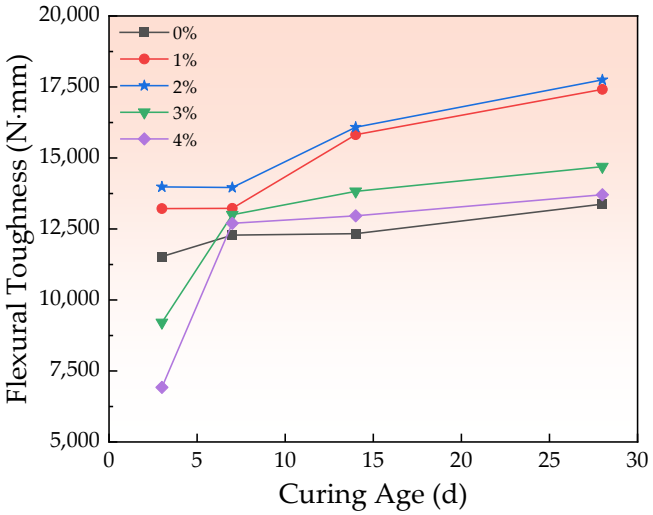


Figure 12. The change in flexural toughness of the RPC at different curing ages.

3.6. Electrochemical Performance Analysis

Figure 13 displays the electrochemical impedance spectroscopy of the RPC cured for 28 days with varying straw fiber contents. The horizontal axis represents the real part, Zr, which represents the AC electrical resistance; the vertical axis represents the imaginary part, -Zi, which represents the capacitance [55]. The AC impedance spectral curve for the specimen's imaginary part first increases, then decreases, aligning with the real part—typical behavior for the EIS of gelled composites. Each curve exhibits an inflection point, where the AC electrical resistance value can, to some extent, indicate the erosion state of the RPC. Additionally, scattered points on the curves arise from polarization and electrophoresis phenomena [56]. The results indicate that the addition of straw fibers could increase the AC electrical resistance of the RPC by rates of 10.17%~58.1%. The maximum AC electrical resistance was observed at a fiber content of 4%.

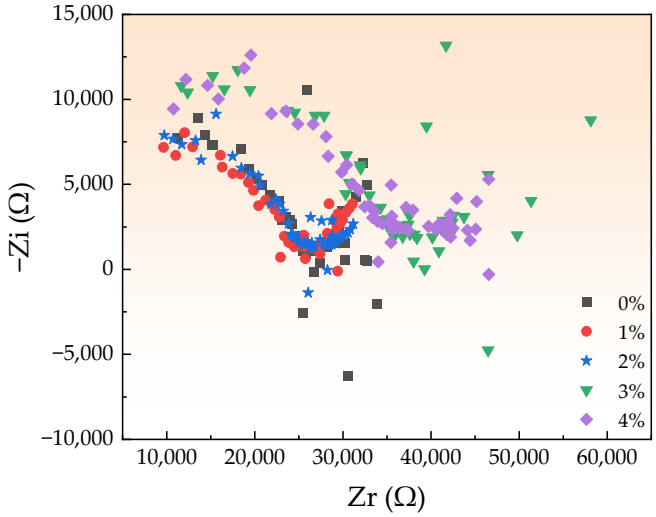


Figure 13. Electrochemical AC impedance spectra of the RPC.

Figure 14 displays the equivalent circuit diagram of the RPC specimen. As depicted, the electrical characteristics of the samples adhered to series conduction models. These models encompassed parallel electrical resistance and capacitance across the pore solution, RPC matrix, and straw fibers, interconnected through electrode contact resistance with the specimens. A comprehensive examination of equivalent circuit diagrams can be found in the studies conducted by Wang et al. [57].

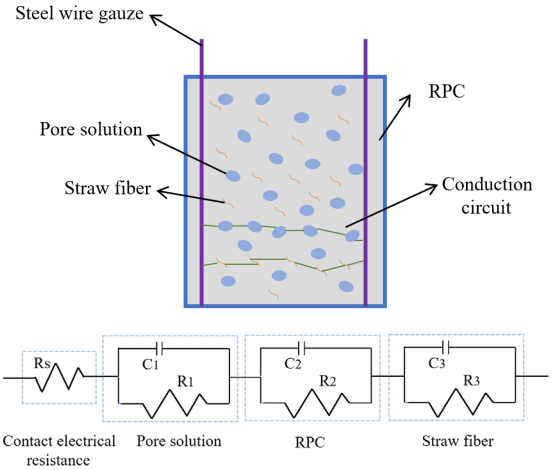


Figure 14. The equivalent circuit diagram for electrochemical properties in the RPC.

Figure 15 depicts the fitting curves of electrical resistance in the RPC with varying straw fiber content throughout the curing period. The electrical resistance of the RPC increased exponentially with curing age, provided the straw fiber content remained constant. The functional relationship can be derived by fitting the data, as demonstrated in Table 3. This phenomenon is attributable to the consumption of pore solution and ions during cement hydration, reducing RPC's conductivity. Cement hydration products filling RPC pores lead to reduced pore size and connectivity, further diminishing conductivity. Only the 1% straw fiber specimens had higher resistance values than the blank specimens. This phenomenon arises from the water absorption characteristics of straw fibers, which decrease the pore solution volume and thereby augment electrical resistance. Moreover, the ion-rich water in straw fibers can create a conductive path, further reducing RPC's electrical resistance [58].

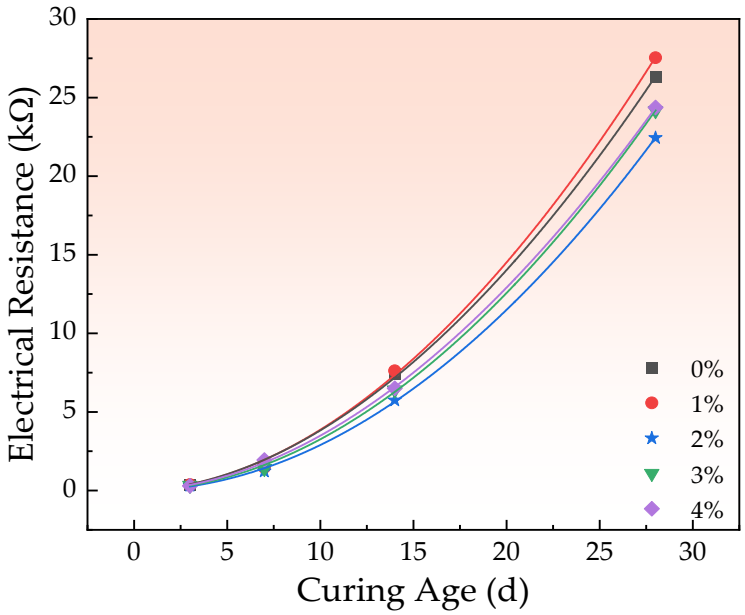


Figure 15. The fitting curve of the RPC electrical resistance with curing age.

Table 3. The fitting function of the RPC electrical resistance with curing age.

Fitting Function	$R = a \cdot t^b$				
	0%	**1%**	**2%**	**3%**	**4%**
A	0.05	0.05	0.03	0.04	0.05
B	1.87	1.91	1.99	1.95	1.88
R^2	0.99	0.99	0.99	0.99	0.99

Figure 16 shows the fitted curves for the mechanical strength and electrical resistance of the RPC. From the figure, it is evident that the flexural and compressive strengths of the RPC rose with the augmentation of electrical resistance. This phenomenon can be attributed to two primary factors: Initially, as RPC hydrates and undergoes curing, the density and bonding strength between the straw fibers and the matrix enhance, consequently boosting the specimen's strength and ductility. In addition, RPC electrical resistance is positively correlated with curing age. This leads to an increase in electrical resistance and an increase in mechanical strengths. Second, the addition of suitable fibers improves the homogeneity of the RPC, increases the electrical conductivity of the material, and enhances fiber bridging and mechanical properties. However, this can result in decreased mechanical strengths of concrete and a rise in the electrical resistance of concrete [59]. The functional relationship can be derived by fitting the data, as demonstrated in Tables 4 and 5.

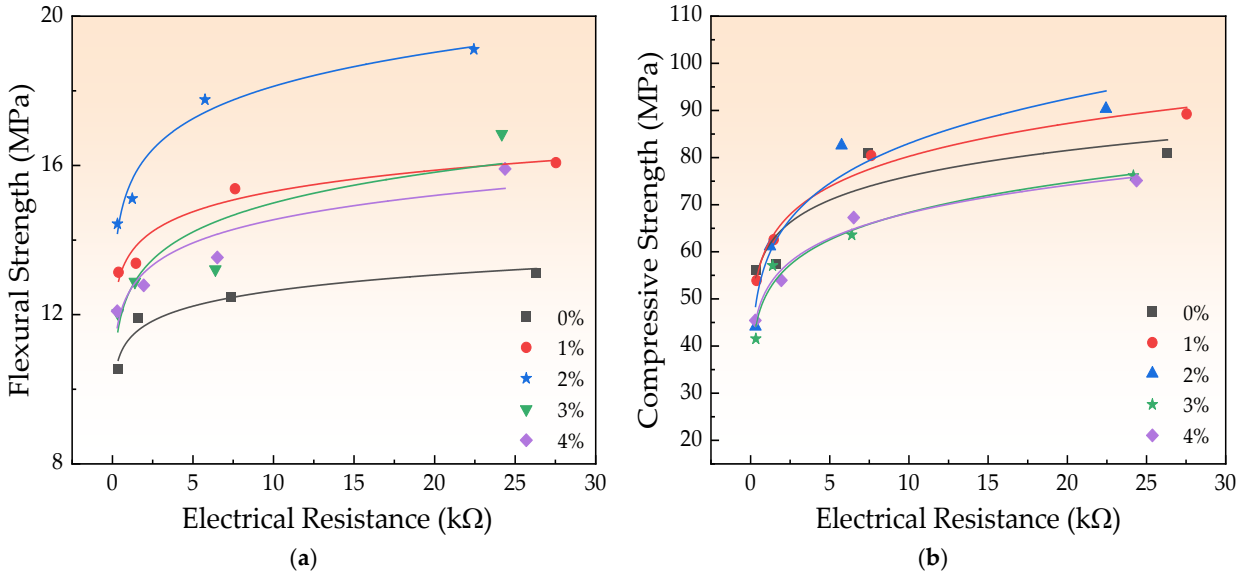


Figure 16. (**a**) The fitting curve of flexural strength of the RPC with electrical resistance; (**b**) the fitting curve of the compressive strength of the RPC with electrical resistance.

Table 4. The fitting function of flexural strength of the RPC with electrical resistance.

Fitting Function	$f_b = a \cdot R^b$				
	0%	1%	2%	3%	4%
a	11.32	13.56	15.39	12.59	12.58
b	0.047	0.05	0.07	0.08	0.06
R^2	0.94	0.94	0.95	0.81	0.88

Table 5. The fitting function of the compressive strength of the RPC with electrical resistance.

Fitting Function	$f_c = a \cdot R^b$				
	0%	1%	2%	3%	4%
a	60.44	60.85	58.01	50.92	51.89
b	0.10	0.12	0.15	0.12	0.12
R^2	0.83	0.98	0.94	0.96	0.98

4. Conclusions

In this experiment, the macroscopic properties of straw fiber RPC before and after chloride salt erosion were investigated. The primary findings of the investigation are outlined below:

Incorporating straw fibers led to decreases in both the slump flow and setting time of fresh RPC by 9.8% to 13.1% and 10.2% to 16.3%, respectively.

The electrical characteristics of straw fiber RPC were simulated by employing series conduction models, which include parallel electrical resistance and capacitance within the pore solution, RPC matrix, and straw fibers. These components were interconnected via contact resistance between the electrodes and the specimens. The addition of straw fibers could augment the AC electrical resistance of the RPC by 10.17%~58.1%. A power function relationship was identified between the electrical resistance of straw fiber RPC and its flexural and compressive strengths.

After 7 days of curing, the incorporation of straw fibers increased flexural strength, compressive strength, and flexural toughness of the RPC by 7.2%~26.7%, −6.17%~8.43%, and 3.36%~13.6%. After 28 days of curing, the incorporation of straw fibers increased flexural strength, compressive strength, and flexural toughness of the RPC by 21.3%~45.76%,

−7.16%~11.62%, and 2.4%~32.7%. The best mechanical properties were obtained with a fiber content of 1% and 2%. Following 10 NaCl dry–wet cycles, the incorporation of straw fibers reduced the loss rates of flexural and compressive strength of the RPC by 9.6%~35.65% and 5.41%~34.88%, respectively, compared to the blank samples.

After subjecting the specimens to 10 cycles of D-A and 200 F-Cs in an NaCl solution, the incorporation of straw fibers resulted in decreased mass loss rates of the RPC by 0.42%~1.68% and 0.89%~1.01%. Similarly, the addition of straw fibers led to reduced rates of ultrasonic velocity loss of the RPC after the same exposure conditions by 2.69%~6.73% and 6.68%~8.9%.

According to the above experimental results, the optimum straw fiber incorporation content in RPC is 1%–2% in a chloride salt erosion environment. This study establishes a characterization relationship between electrical resistance and mechanical strength, which will also contribute to the development of specialized methods for predicting future performance.

Fuzzy logic excels at handling ambiguity and imprecise information; however, it may encounter challenges when faced with extreme conditions or high-dimensional data. Therefore, prior to the experiments, we established hypotheses regarding issues such as consistency of materials, loading conditions, and age-related factors to design our experimental plan. Similarly, while Bayesian networks are powerful in inferring complex dependencies, their effectiveness is highly contingent on the choice of prior probabilities and the quality of the data. Discrepancies between the samples produced in the laboratory and the complexities present in actual engineering scenarios may lead to inaccuracies in the experimental results.

Author Contributions: Conceptualization, H.W. (Hui Wang); methodology, H.W. (Hangyang Wang); software, H.W. (Hangyang Wang); validation, B.C. and K.G.; formal analysis, H.W. (Hangyang Wang); investigation, H.W. (Hangyang Wang) and H.W. (Hui Wang); resources, B.C. and B.X.; data curation, H.W. (Hui Wang); writing—original draft preparation, H.W. (Hangyang Wang); writing—review and editing, H.W. (Hangyang Wang), X.P., K.G. and H.W. (Hui Wang); visualization, H.W. (Hangyang Wang) and H.W. (Hui Wang); supervision, K.G., X.P. and H.W. (Hui Wang); project administration, K.G., X.P. and H.W. (Hui Wang); funding acquisition, H.W. (Hui Wang) and X.P. All authors have read and agreed to the published version of the manuscript.

Funding: This research was supported by Zhejiang Provincial Natural Science Foundation of China (No. LY22E080005, NO. LY24E080010).

Institutional Review Board Statement: Not applicable.

Informed Consent Statement: Not applicable.

Data Availability Statement: The data used to support the findings of this study are available on request.

Conflicts of Interest: Author Bingling Cheng was employed by Ningbo Yonghuan Yuan Environmental Protection Engineering Technology Co., Ltd. Authors Xi Peng and Bin Xu were employed by Ningbo Roaby Technology Industrial Group Co., Ltd. The remaining authors declare that the research was conducted in the absence of any commercial or financial relationships that could be construed as a potential conflict of interest.

References

1. Yusuke, K.; Masaki, M.; Ryuji, N. Verification test of restoration effect of offshore concrete structure using permanent formwork panels and underwater inseparable mortar. *Int. J. Civ. Eng.* **2021**, *19*, 1111–1124.
2. Li, B.; Chen, Z.; Wang, S.; Xu, L. A Review on the Damage Behavior and Constitutive Model of Fiber Reinforced Concrete at Ambient Temperature. *Constr. Build. Mater.* **2024**, *412*, 134919.
3. Wang, Y.; Qiao, P.; Sun, J.; Chen, A. Influence of Fibers on Tensile Behavior of Ultra-High Performance Concrete: A Review. *Constr. Build. Mater.* **2024**, *430*, 136432.
4. Cao, Z.; Wang, K.; Peng, X.; Wang, H.; Huang, R. Influence of NaCl Solution External Erosion on Corrosion Resistance of RPC Reinforced with Straw Fiber. *Coatings* **2023**, *13*, 1308. [CrossRef]
5. Grzymski, F.; Musiał, M.; Trapko, T. Mechanical Properties of Fibre Reinforced Concrete with Recycled Fibres. *Constr. Build. Mater.* **2019**, *198*, 323–331.

6. Esaker, M.; Thermou, G.E.; Neves, L. Impact Resistance of Concrete and Fibre-Reinforced Concrete: A Review. *Int. J. Impact Eng.* **2023**, *180*, 104722.
7. Allam, H.; Duplan, F.; Amziane, S.; Burtschell, Y. Assessment of Manufacturing Process Efficiency in the Dispersion of Carbon Fibers in Smart Concrete by Measuring AC Impedance. *Cem. Concr. Compos.* **2022**, *127*, 104394.
8. Cao, X.; Quan, Y.; Ren, Y.; Fu, F.; Jin, Q.; He, D.; Zheng, Y. Experiment study on reactive powder concrete beams using spirals reinforcement under torsion. *Eng. Struct.* **2023**, *290*, 116361.
9. Ge, W.; Zhang, Z.; Ashour, A.; Li, W.; Jiang, H.; Hu, Y.; Shuai, H.; Sun, C.; Li, S.; Liu, Y. Hydration characteristics, hydration products and microstructure of reactive powder concrete. *J. Build. Eng.* **2023**, *69*, 106306.
10. Liang, Z.; Peng, X.; Wang, H. The Influence of Aspect Ratio of Steel Fibers on the Conductive and Mechanical Properties of Compound Cement Reactive Powder Concrete. *Coatings* **2023**, *13*, 331. [CrossRef]
11. Alharbi, Y.R.; Abadel, A.A.; Salah, A.A.; Mayhoub, O.A.; Kohail, M. Engineering properties of alkali-activated materials reactive powder concrete. *Constr. Build. Mater.* **2021**, *271*, 121550.
12. Hou, X.; Wang, N.; He, T.; Chen, C. Compressive Stress-Strain Relationship of Steam Free Reactive Powder Concrete at Ultra-Low Temperatures. *Cem. Concr. Compos.* **2024**, *152*, 105655.
13. Mayhoub, O.A.; Nasr, E.S.A.; Ali, Y.A.; Kohail, M. The influence of ingredients on the properties of reactive powder concrete: A review. *Ain Shams Eng. J.* **2021**, *12*, 145–158.
14. Richard, P.; Cheyrezy, M. Composition of reactive powder concretes. *Cem. Concr. Res.* **1995**, *25*, 1501–1511.
15. Shafieifar, M.; Farzad, M.; Azizinamini, A. New connection detail to connect precast column to cap beam using ultra-high-performance concrete in accelerated bridge construction applications. *Transp. Res. Rec.* **2018**, *2672*, 207–220.
16. Duan, Y.; Lei, H.; Zhou, Y.; Jin, S. Experimental Study on Bearing Capacity of Compression Members of Space Grid Structures Reinforced by RPC. *Appl. Sci.* **2022**, *12*, 7809. [CrossRef]
17. Ren, P.; Hou, X.; Kodur, V.K.R.; Ge, C.; Zhao, Y.; Zhou, W. Modeling the fire response of reactive powder concrete beams with due consideration to explosive spalling. *Constr. Build. Mater.* **2021**, *301*, 124094.
18. Lai, Z.; Yao, P.; Huang, W.; Chen, B.; Ying, Z. Reactive powder concrete-filled steel tube (RPCFT) members subjected to axial tension: Experimental study and design. *Structures* **2020**, *28*, 933–942.
19. Blunt, J.; Jen, G.; Ostertag, C.P. Enhancing corrosion resistance of reinforced concrete structures with hybrid fiber reinforced concrete. *Corros. Sci.* **2015**, *92*, 182–191.
20. PR, K.R.; Mathangi, D.P.; Sudha, C.; Neelamegam, M. Experimental investigation of reactive powder concrete exposed to elevated temperatures. *Constr. Build. Mater.* **2020**, *261*, 119593.
21. Hiremath, P.; Yaragal, S.C. Performance of polypropelene and polyester fibres-reinforced reactive powder concretes at elevated temperatures. *Constr. Build. Mater.* **2023**, *373*, 130862.
22. Wang, H.; Shi, F.; Shen, J.; Zhang, A.; Zhang, L.; Huang, H.; Liu, J.; Jin, K.; Feng, L.; Tang, Z. Research on the Self-Sensing and Mechanical Properties of Aligned Stainless Steel Fiber-Reinforced Reactive Powder Concrete. *Cem. Concr. Compos.* **2021**, *119*, 104001.
23. Branston, J.; Das, S.; Kenno, S.Y.; Taylor, C. Mechanical Behaviour of Basalt Fibre Reinforced Concrete. *Constr. Build. Mater.* **2016**, *124*, 878–886.
24. Zhang, G.Z.; Liu, C.; Cheng, P.F.; Li, Z.; Han, Y.; Wang, X.Y. Enhancing the Interfacial Compatibility and Self-Healing Performance of Microbial Mortars by Nano-SiO_2-Modified Basalt Fibers. *Cem. Concr. Compos.* **2024**, *152*, 105650.
25. Le, D.L.; Salomone, R.; Nguyen, Q.T. Circular Bio-Based Building Materials: A Literature Review of Case Studies and Sustainability Assessment Methods. *Build. Environ.* **2023**, *244*, 110774.
26. Le, D.L.; Salomone, R.; Nguyen, Q.T.; Versele, A.; Piccardo, C. Status and Barriers to Circular Bio-Based Building Material Adoption in Developed Economies: The Case of Flanders, Belgium. *J. Environ. Manag.* **2024**, *367*, 121965.
27. Singh, A.K.; Bedi, R.; Khajuria, A. A review of composite materials based on rice straw and future trends for sustainable composites. *J. Clean. Prod.* **2024**, *457*, 142417.
28. Wu, B.; Zhang, S.; Zhao, Y. Dynamic compressive properties of rubberized mortar reinforced with straw-fiber additive. *Constr. Build. Mater.* **2023**, *408*, 133679.
29. Basta, A.H.; Lotfy, V.F.; Shafik, E.S. Synergistic Valorization of Rice Straw and Red Brick Demolition in development performance of Lightweight Cement Mortars. *J. Build. Eng.* **2024**, *92*, 109769.
30. Ahmad, J.; Mohammed, J.; Tayyab, N.M. Improvement in the strength of concrete reinforced with agriculture fibers: Assessment on mechanical properties and microstructure analysis. *J. Eng. Fibers Fabr.* **2024**, *19*, 1226480.
31. Wu, Z.; Wang, X.; Chen, Z. Experimental study on Corn Straw Fiber (CSF) toughening EPS concrete. *Constr. Build. Mater.* **2024**, *429*, 136325.
32. Fu, Z.; Wang, X.; Yang, W.; Ren, J.; Dong, B.; Xing, F. Enhanced Repetitive Self-Healing of Cementitious Materials through Modified Biochar and Optimised Superabsorbent Polymer. *Constr. Build. Mater.* **2024**, *443*, 137716.
33. Alioui, A.; Kaitouni, S.I.; Azalam, Y.; Bendada, E.M.; Mabrouki, M. Effect of Straw Fibers Addition on Hygrothermal and Mechanical Properties of Carbon-Free Adobe Bricks: From Material to Building Scale in a Semi-Arid Climate. *Build. Environ.* **2024**, *255*, 111380.
34. Nian, T.; Li, P.; Ge, J.; Song, J.; Wang, M. Green Environmental Protection and Sustainable Utilization of Straw: Investigation for Molecular Dynamics of Highland Barley Straw Fiber to Enhancing Road Performance of Asphalt. *J. Clean. Prod.* **2024**, *452*, 141940.

35. Jin, Z.; Mao, S.; Zheng, Y.; Liang, K. Pre-Treated Corn Straw Fiber for Fiber-Reinforced Concrete Preparation with High Resistance to Chloride Ions Corrosion. *Case Stud. Constr. Mater.* **2023**, *19*, e02368.
36. Wu, H.; Shen, A.; Cheng, Q.; Cai, Y.; Ren, G.; Pan, H.; Deng, S. A review of recent developments in application of plant fibers as reinforcements in concrete. *J. Clean. Prod.* **2023**, *419*, 138265.
37. Zhang, L.; Huang, M.; Yang, F.; Zhang, W. A Novel Hydrophilic Modification Method of EPS Particles: Conception Design and Performances in Concrete. *Cem. Concr. Comp.* **2023**, *142*, 105199.
38. Ma, J.; Yuan, H.; Zhang, J.; Zhang, P. Enhancing Concrete Performance: A Comprehensive Review of Hybrid Fiber Reinforced Concrete. *Structures* **2024**, *64*, 106560.
39. Luo, J.; Quan, Z.; Shao, X.; Li, F.; He, S. Mechanical Performance of RPC and Steel–RPC Composite Structure with Different Fiber Parameters: Experimental and Theoretical Research. *Polymers* **2022**, *14*, 1933. [CrossRef] [PubMed]
40. Shi, X.; Ning, B.; Wang, J.; Cui, T.; Zhong, M. Improving Flexural Toughness of Foamed Concrete by Mixing Polyvinyl Alcohol-Polypropylene Fibers: An Experimental Study. *Constr. Build. Mater.* **2023**, *400*, 132689.
41. Bortoletto, M.; Sanches, A.O.; Santos, J.A.; da Silva, R.G.; Tashima, M.M.; Payá, J.; Soriano, L.; Borrachero, M.V.; Malmonge, J.A.; Akasaki, J.L. New Insights on Understanding the Portland Cement Hydration Using Electrical Impedance Spectroscopy. *Constr. Build. Mater.* **2023**, *407*, 133566.
42. Meng, Z.; Liu, Q.; She, W.; Cai, Y.; Yang, J.; Farjad Iqbal, M. Electrochemical Deposition Method for Load-Induced Crack Repair of Reinforced Concrete Structures: A Numerical Study. *Eng. Struct.* **2021**, *246*, 112903.
43. Ojala, T.; Ahmed, H.; Kuusela, P.; Seppänen, A.; Punkki, J. Monitoring of Concrete Segregation Using AC Impedance Spectroscopy. *Constr. Build. Mater.* **2023**, *384*, 131453.
44. de Almeida, E.F., Jr.; Martini, S. Measurements of Electrical Impedance in Cementitious Mortars: Influence of Electrodes and Physical Dimensions of Specimens. *Case Stud. Constr. Mater.* **2023**, *18*, e01880.
45. Gong, K.; Liang, Z.; Peng, X.; Wang, H. Research into Preparation and Performance of Fast-Hardening RPC Mixed with Straw. *Materials* **2023**, *16*, 5310. [CrossRef] [PubMed]
46. Liu, J.; Xie, X.; Li, L. Experimental Study on Mechanical Properties and Durability of Grafted Nano-SiO_2 Modified Rice Straw Fiber Reinforced Concrete. *Constr. Build. Mater.* **2022**, *347*, 128575.
47. Tai, Y.; Yang, L.; Gao, D.; Kang, K.; Cao, Z.; Zhao, P. Properties Evolution and Deterioration Mechanism of Steel Fiber Reinforced Concrete (SFRC) under the Coupling Effect of Carbonation and Chloride Attack. *J. Build. Eng.* **2024**, *95*, 110275.
48. Tu, Y.; Liu, D.; Yuan, L.; Zhang, Y. Corrosion Resistance of Concrete Strengthened with Fibre-Reinforced Polymer Sheets. *Mag. Concr. Res.* **2022**, *74*, 54–69.
49. Wang, H.; Jin, K.; Zhang, A.; Zhang, L.; Han, Y.; Liu, J.; Shi, F.; Feng, L. External Erosion of Sodium Chloride on the Degradation of Self-Sensing and Mechanical Properties of Aligned Stainless Steel Fiber Reinforced Reactive Powder Concrete. *Constr. Build. Mater.* **2021**, *287*, 123028.
50. Marcos-Meson, V.; Michel, A.; Solgaard, A.; Fischer, G.; Edvardsen, C.; Skovhus, T.L. Corrosion Resistance of Steel Fibre Reinforced Concrete-A Literature Review. *Cem. Concr. Res.* **2018**, *103*, 1–20.
51. Abolhasani, A.; Nazarpour, H.; Dehestani, M. The Fracture Behavior and Microstructure of Calcium Aluminate Cement Concrete with Various Water-Cement Ratios. *Theor. Appl. Fract. Mech.* **2020**, *109*, 102690.
52. Ammari, M.S.; Belhadj, B.; Bederina, M.; Ferhat, A.; Quéneudec, M. Contribution of Hybrid Fibers on the Improvement of Sand Concrete Properties: Barley Straws Treated with Hot Water and Steel Fibers. *Constr. Build. Mater.* **2020**, *233*, 117374.
53. Su, Q.; Xu, J. Mechanical Properties of Concrete Containing Glass Sand and Rice Husk Ash. *Constr. Build. Mater.* **2023**, *393*, 132053.
54. Zhang, Y.; Wang, J.; Wang, J.; Qian, X. Preparation, Mechanics and Self-Sensing Performance of Sprayed Reactive Powder Concrete. *Sci. Rep.* **2022**, *12*, 7787.
55. Miyazaki, Y.; Nakayama, R.; Yasuo, N.; Watanabe, Y.; Shimizu, R.; Packwood, D.M.; Nishio, K.; Ando, Y.; Sekijima, M.; Hitosugi, T. Bayesian Statistics-Based Analysis of AC Impedance Spectra. *AIP Adv.* **2020**, *10*, 045231.
56. Valcuende, M.; Lliso-Ferrando, J.R.; Ramón-Zamora, J.E.; Soto, J. Corrosion Resistance of Ultra-High Performance Fibre-Reinforced Concrete. *Constr. Build. Mater.* **2021**, *306*, 124914.
57. Wang, H.; Du, T.; Zhang, A.; Cao, P.; Zhang, L.; Gao, X.; Liu, J.; Shi, F.; He, Z. Relationship between Electrical Resistance and Rheological Parameters of Fresh Cement Slurry. *Constr. Build. Mater.* **2020**, *256*, 119479.
58. Xu, Z.; Cao, P.; Wang, D.; Wang, H. The Corrosion Resistance of Reinforced Magnesium Phosphate Cement Reactive Powder Concrete. *Materials* **2022**, *15*, 5692. [CrossRef] [PubMed]
59. Wang, H.; Cai, X.; Rao, C.; Wang, K.; Wang, J. Mechanical and Electrical Properties of Rapid-Strength Reactive Powder Concrete with Assembly Unit of Sulphoaluminate Cement and Ordinary Portland Cement. *Materials* **2022**, *15*, 3371. [CrossRef]

Disclaimer/Publisher's Note: The statements, opinions and data contained in all publications are solely those of the individual author(s) and contributor(s) and not of MDPI and/or the editor(s). MDPI and/or the editor(s) disclaim responsibility for any injury to people or property resulting from any ideas, methods, instructions or products referred to in the content.